J Therm Anal Calorim (2014) 118:1569–1575
DOI 10.1007/s10973-014-4085-8

Using TG–FTIR and TG–MS to study thermal degradation of metal hypophosphites

Weihong Wu · Shufang Lv · Xin Liu · Hongqiang Qu · Hongchao Zhang · Jianzhong Xu

Received: 28 April 2014 / Accepted: 9 August 2014 / Published online: 29 August 2014

Abstract Three typical metal hypophosphite flame retardants $La(H_2PO_2)_3{\cdot}H_2O$ (LHP), $Ce(H_2PO_2)_3{\cdot}H_2O$ (CHP), and $Al(H_2PO_2)_3$ (AHP) were synthesized and characterized by Fourier transform infrared spectroscopy (FTIR), X-ray powder diffraction, scanning electron microscopy, thermogravimetric analysis (TG), derivative thermogravimetric analysis, and differential thermal analysis. The thermal degradation products from the synthesized metal hypophosphites were also investigated using thermogravimetry coupled with Fourier transform infrared spectroscopy (TG–FTIR) and thermogravimetry coupled with mass spectrometry (TG–MS). The synthesized metal hypophosphites were also used as flame retardants for poly (1,4-butylene terephthalate) (PBT), and the combustion properties of flame-retarded PBT were evaluated using the limiting oxygen index and UL-94 tests. The results showed that the metal hypophosphites LHP, CHP, and AHP can be used as effective flame retardants for PBT, and these compounds can be obtained through a simple precipitation method. TG–FTIR and TG–MS results showed that the degradation process of AHP involves two steps, corresponding to the removal PH_3 reaction and the further dehydration reaction of the hydrogen phosphate aluminum. While LHP and CHP have three degradation steps, the additional step is due to that LHP and CHP which will loss the crystal water at lower temperature.

W. Wu
College of Science, Agriculture University of Hebei, Baoding 071000, People's Republic of China

S. Lv · X. Liu · H. Qu (✉) · H. Zhang · J. Xu
College of Chemistry and Environmental Science, Hebei University, No. 180 Wusi East Road, Baoding 071002, Hebei, People's Republic of China
e-mail: hqqu@163.com

Keywords Metal hypophosphite · Flame retardant · TG–FTIR · TG–MS · Thermal analysis

Introduction

Metal hypophosphite compounds, such as aluminum hypophosphite (AHP), magnesium hypophosphite, and cerium hypophosphite have attracted much attention over the decades for their high thermal and chemical stabilities, good mechanical and electrical properties, and environmentally friendly properties [1–3]. Especially, AHP as a novel class of phosphorous-based flame retardants, which is expected as a promising candidate for replacing halogen-based flame retardants, also it has been applied in the treatment of organic materials such as glass-filled polyamide 6 [3], polybutylene terephthalate (PBT) [4, 5], poly(ethylene terephthalate) [6], and polylactide [7]. These publications have described the flame retardancy and speculated the thermal degradation mechanism of the metal hypophosphites. However, many of these reports are in lack of detailed study of the thermal degradation of the metal hypophosphites. Therefore, to clarify the thermal degradation processes of these metal hypophosphites is of great significance to the study of the flame-retardant mechanism of these compounds in different polymers and to expand their applications.

Thermogravimetry analysis is a simple, convenient, fast, and effective method for the study of pyrolysis and flame retardants [8–11]. Especially, thermogravimetry–Fourier transform infrared spectroscopy (TG–FTIR) and thermogravimetry–mass spectrometry analysis (TG–MS) are very useful methods to confirm the content and species of the gaseous products of the thermal decomposition [12, 13]; the results of these methods would be helpful to develop a

better understanding of the actions of flame retardants and thus facilitate the development of new flame retardants.

The aim of this work is to synthesize a series of metal hypophosphite compounds, which are characterized by Fourier transform infrared spectroscopy (FTIR), X-ray diffraction (XRD), scanning electron microscopy (SEM), thermogravimetric analysis (TG), derivative thermogravimetric analysis (DTG) and differential thermal analysis (DTA). The gaseous products of the thermal degradation process were studied using TG–FTIR and TG–MS. The flame retardancy of metal hypophosphites in PBT was also studied using the limiting oxygen index (LOI) and UL-94 tests.

Experimental

Materials

The materials used in synthesis of metal hypophosphite compounds include sodium hypophosphite ($NaH_2PO_2{\cdot}H_2O$) (Tianjin Kemiou Chemicals Co. Ltd, Tianjin, China), crystallization of aluminum chloride ($AlCl_3{\cdot}6H_2O$) (Shanghai Jinshan Chemicals Co. Ltd, Shanghai, China), lanthanum chloride ($LaCl_3{\cdot}7H_2O$) (Tianjin Guangfu Chemical Research Institute, Tianjin, China), cerium chloride ($CeCl_3{\cdot}7H_2O$) (Tianjin Guangfu Chemical Research Institute, Tianjin, China), potassium chloride (KCl) (Tianjin Taixin Chemicals Co. Ltd, Tianjin, China), and concentrated hydrochloric acid (HCl) (Tianjin Kemiou Chemicals Co. Ltd, Tianjin, China). They are all of A.R. grade and used directly without further purification. PBT (B4500) was purchased from BASF Chemical Company, Germany.

Preparation of samples

Synthesis of $La(H_2PO_2)_3 \cdot H_2O$ *(LHP) [14]*

19.08 g (0.18 mol) $NaH_2PO_2{\cdot}H_2O$ was dissolved in pH 1.4 (KCl–HCl) buffer solution (30 mL). The solvent used for the buffer solution was deionized water. 22.29 g (0.06 mol) $LaCl_3{\cdot}7H_2O$ in the buffer solution (50 mL) was added slowly. The reaction mixture was heated to 40 °C under reflux in a nitrogen atmosphere for 3 h. The resulting solid was collected by suction filtration, washed with deionized water and ethanol, and then dried to constant mass in a vacuum oven at 80 °C. The yield was 69.5 %.

Synthesis of $Ce(H_2PO_2)_3 \cdot H_2O$ *(CHP) [14]*

19.08 g (0.18 mol) $NaH_2PO_2{\cdot}H_2O$ was dissolved in pH 1.4 (KCl–HCl) buffer solution (30 mL). The solvent used for the buffer solution was deionized water. 22.35 g (0.06 mol) $CeCl_3{\cdot}7H_2O$ in the buffer solution (50 mL) was added slowly. The reaction mixture was heated to 40 °C under reflux in a nitrogen atmosphere for 3 h. The resulting solid was collected by suction filtration, washed with deionized water and ethanol, and then dried to constant mass in a vacuum oven at 80 °C. The yield was 72.4 %.

Synthesis of $Al(H_2PO_2)_3$ *(AHP)*

25.44 g (0.24 mol) $NaH_2PO_2{\cdot}H_2O$ and 30 mL of deionized water were added to a 250 mL three-necked flask, and then, the mixture was stirred for 15 min at 50 °C. After the solution became transparent, the temperature of the system was elevated to 85 °C for 30 min. The solution (30 mL), which contained 19.27 g (0.08 mol) $AlCl_3{\cdot}6H_2O$, was dropped into the reaction mixture slowly, and then, a white precipitate appeared. The reaction system was stirred at the same temperature for 1 h, and then, the target product was filtered at room temperature, washed with distilled water and ethanol, and dried to constant mass in a vacuum oven at 80 °C. The yield was 88.4 %.

Preparation of flame retardant PBT samples

PBT and all additives were dried at 80 °C overnight before use. The formulations were melting and blended using a twin-screw extruder (SHJ-20, Nanjing Giant Machinery CO., Ltd, China). The temperatures of the five zones were 220, 220, 225, 225, and 225 °C, respectively. Extruded materials were pelletized and dried. The chips were injected and molded into standard specimen using micro-injection molding machine (SZ-15, Wuhan Ruiming plastic Machinery CO., Ltd, China). The temperatures of the melt and mold were 230 and 40 °C, respectively, and the pressure of injection was 0.4 MPa. Also, the chips were molded using a hot press at 225 °C in order to obtain 3-mm-thick plaques.

Characterization

The products were analyzed by Fourier transform infrared spectra spectroscopy (Bruker, TENSOR27 FTIR spectrophotometer, Germany).

The structure of the sample was performed by XRD (Bruker, D8-ADVANCE X-ray diffractometer, Germany) with Cu Ka radiation ($\lambda = 1.542$ Å, $2\theta = 25°$–$70°$) at the scanning rate of 0.01°/s. Scherrer method was used to evaluate the crystalline size, and equation is shown as follow [15]:

$$D = \frac{K\lambda}{\beta \cos\theta}, \quad (1)$$

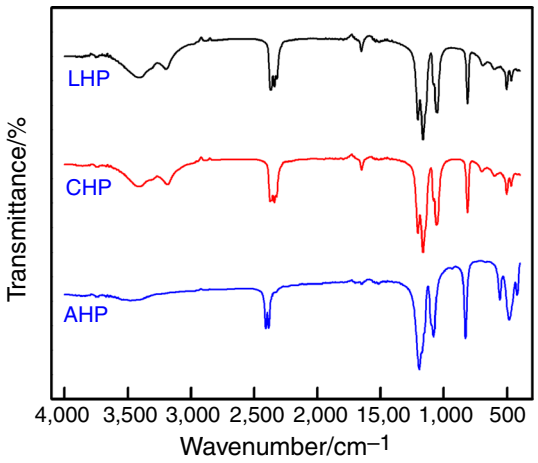

Fig. 1 FTIR spectra of the metal hypophosphites

where λ is the wavelength of X-ray radiation, K is a constant taken as 0.89, θ is the diffraction angle, and β is the full width at half maximum (FWHM)).

The morphology of the samples was characterized by SEM (Hitachi, TM3000 SEM, Japan) at acceleration voltage of 15 kV.

TG, DTG, and DTA were performed on a Netzsch Co. Ltd. TG 449C thermogravimeter (Germany) with a heating rate of 10 °C min^{-1} under nitrogen atmosphere flow rate of 60 mL min^{-1}. The temperature ranged from room temperature to 800 °C.

TG–FTIR measurements were carried out on a Netzsch Co. Ltd. TG 449 C thermogravimeter (Germany) coupled with a Bruker TENSOR27 FTIR spectrophotometer (Germany). About 8 ± 0.2 mg of each sample was heated from ambient temperature up to 800 °C with a heating rate of 10 °C min^{-1} under high purity argon (flow rate = 60 mL min^{-1}). The coupling system between the TG and FTIR was a quartz capillary kept at a temperature of 200 °C.

A TG–MS instrument (STA 449 C-QMS 403 C, Netzsch Co. Ltd., Germany) was used for analyzing fragments from the thermobalance was performed in high purity argon (99.999 %) at a flow rate of 60 mL min^{-1}. In the experiment, a sample weighing approximately 8 ± 0.2 mg was heated at 10 °C min^{-1} from ambient temperature up to 800 °C. Mass analysis was carried out using a spectrometer with an electronimpact ion source (70 eV); energy scanning was carried out in the range *m/z* 10–150 at the rate of 0.2 s^{-1} for each mass unit. The connection between the thermobalance and the mass spectrometer was also done by means of a quartz capillary at 200 °C.

LOI values were determined in accordance with ASTM D2863-2000 using a JF-3 oxygen index meter (Jiangning Analytical Instrument Factory, China).

Table 1 Assignment of some main absorbance bands in the FTIR spectra

Wavenumber/cm^{-1}	Assignment
3,460–3,230	O–H stretching vibrations
2,450–2,300	PH_2 stretching modes
1,632	H_2O bending vibration
1,250–1,100	PH_2 bending modes
1,079	P–O modes
809	Rocking mode of PH_2

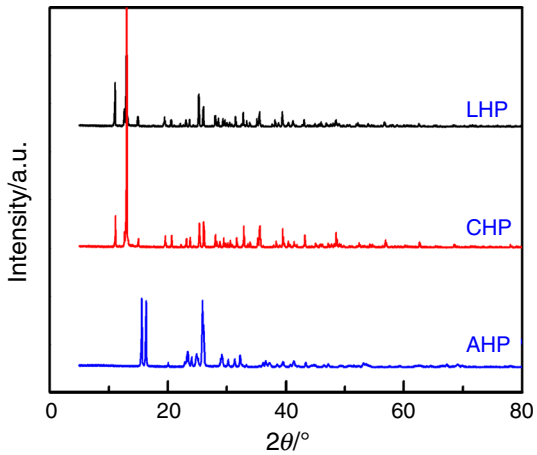

Fig. 2 XRD patterns of metal hypophosphites

UL-94 test was carried out using a CZF-3 vertical flammability tester (Jiangning Analytical Instrument Factory, China) according to ASTM D3801-2006.

Results and discussion

Characterization of metal hypophosphites

FTIR spectra of the metal hypophosphites are presented in Fig. 1. The band assignments for the FTIR spectra of the groups in metal hypophosphites are summarized in Table 1.

The bands in the region of 3,230–3,460 cm^{-1} observed in the compounds of LHP and CHP are attributed to O–H stretching vibrations [16]. The weak peak at 1,632 cm^{-1} is attributed to the bending vibration of H_2O. These results indicate that water molecules exist in the two compounds. However, in the infrared spectra of AHP the characteristic bands of water molecules are not present, indicating that the compound is anhydrous. The bands in the region of 2,300–2,450 cm^{-1} observed in all the metal hypophosphites are attributed to PH_2 stretching modes [16]. The bands between 1,100 and 1,250 cm^{-1} are in correspondence to

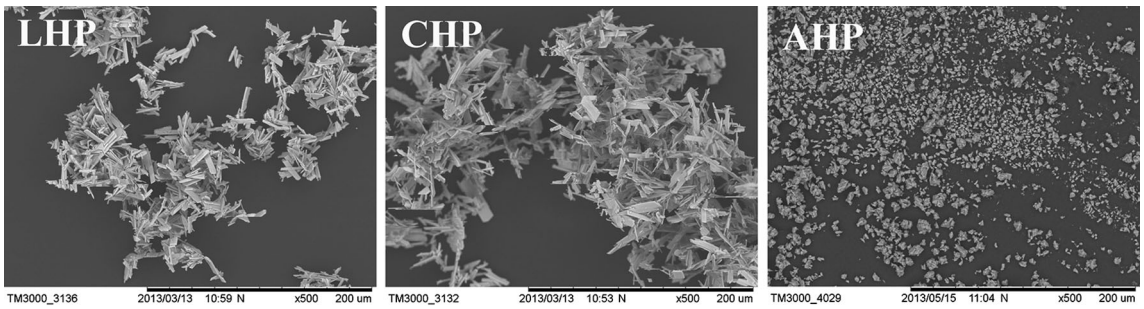

Fig. 3 SEM micrographs of synthesized metal hypophosphites

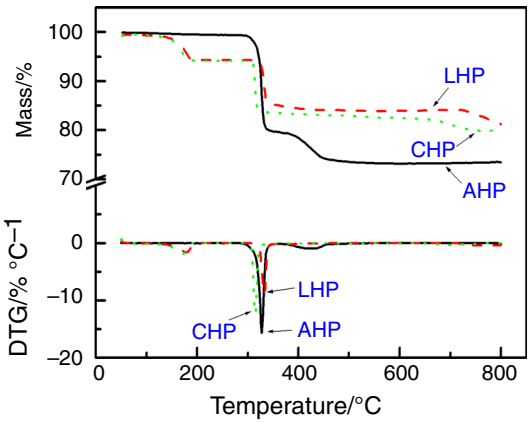

Fig. 4 TG/DTG curves of the metal hypophosphites in N_2 atmosphere

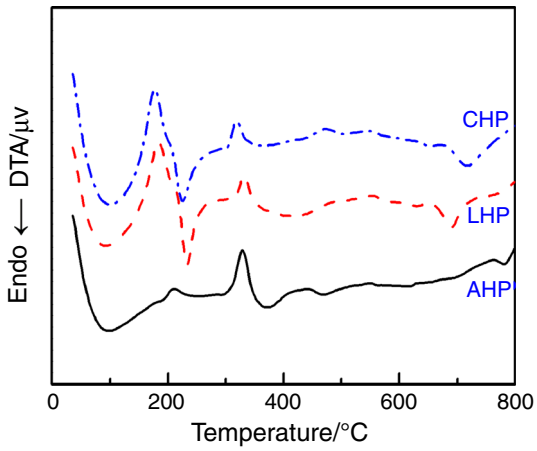

Fig. 5 DTA curves of the metal hypophosphites in N_2 atmosphere

the bending modes of PH_2 [17]. The medium intensity peak at 809 cm^{-1} is assigned to the rocking mode of PH_2. The weak peak at 1,079 cm^{-1} is attributed to P–O modes.

The XRD patterns of the prepared metal hypophosphites are shown in Fig. 2. All detectable peaks of the metal hypophosphites are indexed as synthesized $La(H_2PO_2)_3{\cdot}H_2O$, $Ce(H_2PO_2)_3{\cdot}H_2O$, and $Al(H_2PO_2)_3$, which are identified using the standard data of PDF # 140577 and the literatures [14, 18], respectively.

The average crystallite sizes of LHP, CHP, and AHP, determined from X-ray line broadening using the Debye–Scherrer's formula, are 88, 94, and 58 nm, respectively.

SEM micrographs of the synthesized metal hypophosphites are shown in Fig. 3. SEM micrographs of LHP and CHP illustrate some small laminar crystals, in the sizes of about 10–20 μm in length and 3–8 μm in width, while the lamellae of the crystals shows re-texturing and coalescence in aggregates of irregularly shaped crystals, as a result, the particle size of LHP and CHP has increased obviously. The morphology of the prepared AHP shows irregular granular size in the range of 1–5 μm.

The thermal stability is very important to flame retardant, and the thermal degradation behavior is a great concern also. TG, DTG, and DTA curves of the metal hypophosphites in N_2 are shown in Figs. 4 and 5, respectively.

TG and DTG curves of AHP can be divided into two stages. The first stage (Step I) of decomposition is from 298 to 381 °C, and the mass loss in this step is 20.69 % with the maximal mass loss rate at 325.6 °C. The second stage (Step II) lies in the temperature range of 382–511 °C, and the mass loss in this step is 6.07 % with the maximal mass loss rate at 423.7 °C. Wei Yang et al. speculated that the decomposition process of AHP could be represented by two equations as detailed below [6]:

$$2Al(H_2PO_2)_3 \xrightarrow{\Delta} Al_2(HPO_4)_3 + 3PH_3. \quad (2)$$

$$2Al_2(HPO_4)_3 \xrightarrow{\Delta} Al_4(P_2O_7)_3 + 3H_2O \quad (3)$$

If we calculate the mass loss of AHP in the two stages according to the decomposition process above, we can find that the calculative results and the experimental results are basically identical. The specific data are shown in Table 2. TG and DTG curves of LHP and CHP are very similar and can be divided into three stages. The first stage (Step I) of decomposition is from 117 to 191 °C. The second stage (Step II) lies in the temperature range of 300–434 °C. This

Table 2 The mass loss of metal hypophosphites in the three stages

Sample	Mass loss in step I/%		Mass loss in step II/%		Mass loss in step III/%	
	Experimental	Calculative	Experimental	Calculative	Experimental	Calculative
LHP	5.16	5.12	12.93	14.49	3.63	3.84
CHP	5.33	5.10	14.29	14.44	3.18	3.82
AHP	20.69	22.98	6.07	6.09		

is followed by the third and the final stage (Step III) of decomposition between 638 and 800 °C.

As shown in Table 2, by comparing the experimental and calculative mass loss results of the three stages, the decomposition process of LHP and CHP could be represented by three equations as detailed below (M = La or Ce):

$$M(H_2PO_2)_3 \cdot H_2O \xrightarrow{\Delta} M(H_2PO_2)_3 + H_2O \quad (4)$$

$$2M(H_2PO_2)_3 \xrightarrow{\Delta} M_2(HPO_4)_3 + 3PH_3 \quad (5)$$

$$2M_2(HPO_4)_3 \xrightarrow{\Delta} M_4(P_2O_7)_3 + 3H_2O \quad (6)$$

DTA curve of AHP exhibits an exothermic peak and an endothermic peak around 328 and 460.0 °C, respectively. The exothermic peak can be attributed to the removal of PH_3 reaction of AHP, and the endothermic peak corresponds to the further dehydration reaction of the hydrogen phosphate aluminum. Moreover, two endothermic peaks and an exothermic peak on DTA curves of LHP and CHP are observed at about 230, 700, and 330 °C, which correspond to the three stages in TG curves of LHP and CHP.

TG–FTIR analysis

In order to gain the information of the degradation products in gas phase, the evolved gases of the samples from TG furnace were inspected by simultaneous FTIR. Figures 6, 7, and 8 show FTIR spectra of AHP, LHP, and CHP for the gas products at different temperatures. As shown in Fig. 6, corresponding to TG and DTG results, the infrared absorption for the gases produced from thermal degradation of AHP began to appear at about 300 °C, and at 328 °C the characteristic peaks of PH_3 at 2,319 and 988 cm^{-1} have the highest intensity [19], and then the intensity of the characteristic absorption gradually decreased. At 353 °C, the characteristic peaks of H_2O at 1300, 1665, 3,500–4,000 cm^{-1} began to appear, and the intensity also showed in a route increase firstly and then decrease in variation. These results indicate that PH_3 gases have been generated first in gas products, and then the water molecules were generated in the decomposition process of AHP.

For LHP and CHP, as shown in Figs. 7 and 8, H_2O began to appear at about 132 °C, its concentration

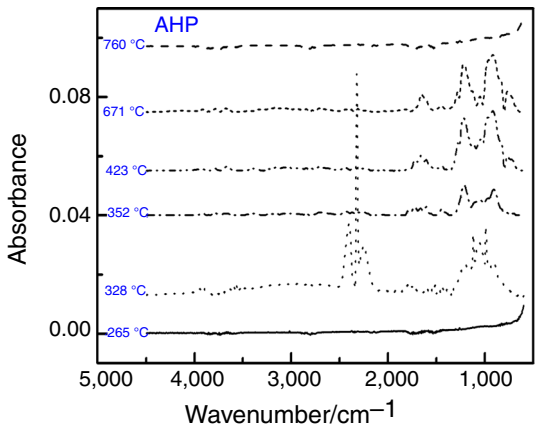

Fig. 6 FTIR spectra of AHP under different pyrolysis temperatures

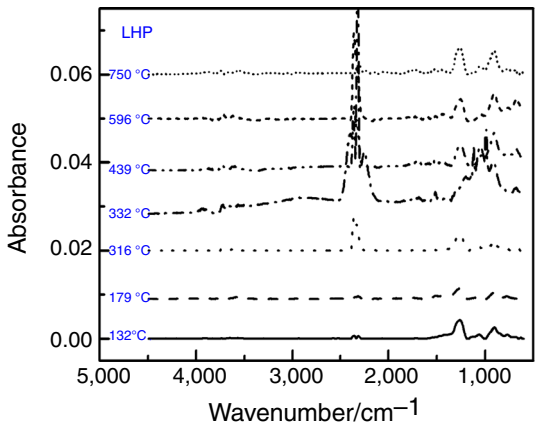

Fig. 7 FTIR spectra of LHP under different pyrolysis temperatures

gradually increased up to about 179/171 °C, at which a maximum was reached; thereafter, the amount of H_2O decreased rapidly. At about 316/240 °C, the characteristic peaks of PH_3 began to appear, and at about 332/314 °C, the maximum value was reached. Compared with the first dehydration reaction, the second dehydration reaction of LHP and CHP becomes more difficult, and only after 587/596 °C another water molecule was released from LHP and CHP.

In conclusion, the gaseous products released during the two degradation stages of AHP were PH_3 and H_2O.

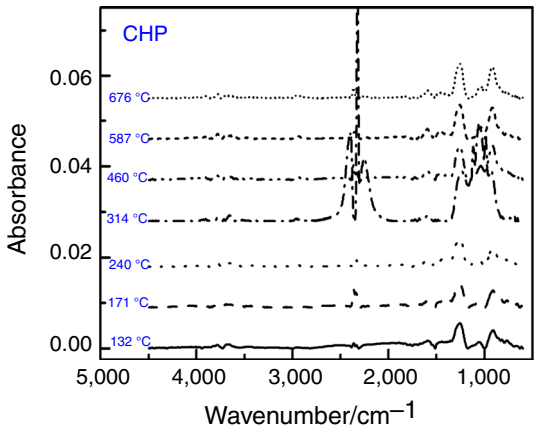

Fig. 8 FTIR spectra of CHP under different pyrolysis temperatures

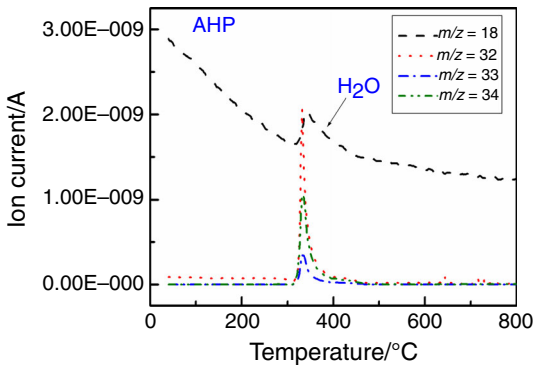

Fig. 9 MS results of the AHP

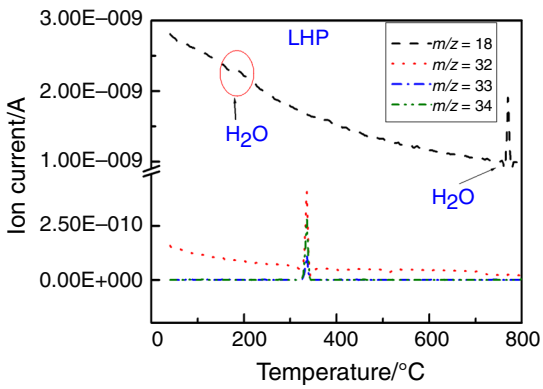

Fig. 10 MS results of the LHP

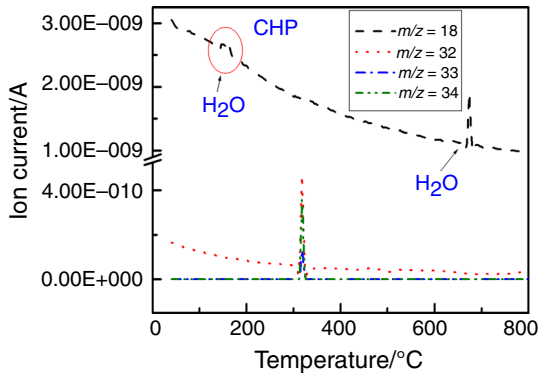

Fig. 11 MS results of the CHP

Compared with AHP, it was found that in case of LHP and CHP, the removal of the crystallization water occurs first, and then further decomposition occurs to form PH_3 as gas product, and the final dehydration reaction for the acid phosphate can only be carried out at elevated temperature. Detailed analysis on the yield of different gases generated during pyrolysis was conducted using TG–MS studies.

TG–MS analysis

Because FTIR measurement investigates only qualitative information about the functional group of different pyrolysis products, MS was performed to recognize the accurate composition of the pyrolysis products. It can be observed from Figs. 9, 10, and 11 that intensive signals of the species with different mass-to-charge (m/z) ratios appear with the degradation stage described as TG–FTIR. MS signals at $m/z = 18$ indicated the presence of H_2O [20], while PH_3 was determined by MS signals corresponding to $m/z = 34$, 33, 32. These results obtained from TG–MS strongly supported the conclusions derived from TG–FTIR analysis.

Compared with AHP, MS signal intensity of LHP and CHP at $m/z = 18$ is lower, which is due to the relatively smaller mass loss. Accordingly, MS signals of CHP and LHP at $m/z = 18$ can be clearly detected corresponding to the first and the third mass loss stage.

Flame-retardant properties

The metal hypophosphites, AHP, LHP, and CHP, were used as flame retardants for PBT, and LOI and UL-94 tests were performed to investigate the flame retardancy of each formulation, which are summarized in Table 3. As shown in Table 3, PBT is a flammable polymeric material with the LOI of 19.8 %, and in UL-94 test, burning PBT was not extinguishable, and there was serious dripping in the first stage of the combustion. LOI value increased from 19.8 to 27.8 % when 25 mass% AHP was present, and the combustion behavior of PBT composite was further influenced, and a V-1 rating was achieved. Compared with AHP, LHP and CHP have little difference affect on LOI for flame retardant PBT. However, when 25 mass% LHP was present, the PBT/LHP (75/25) sample can achieve V-0 rating.

Table 3 The combustibility of flame-retarded PBT

Samples	LOI/%	UL 94
PBT	19.8	–
PBT/AHP (75/25)	27.8	V-1
PBT/LHP (75/25)	26.8	V-0
PBT/CHP (75/25)	27.7	V-2

This suggests that LHP can effectively enhance the dripping resistant performance of PBT.

Conclusions

AHP, LHP, and CHP were synthesized by a relatively easy method. Synthesized AHP, LHP, and CHP were confirmed by TG/DTG/DTA, SEM, XRD, and FTIR measurements. TG–FTIR and TG–MS results showed that the thermal degradation of AHP occurs in two stages. The first stage is the removal PH_3 reaction of AHP, and the second stage is the further dehydration reaction of the hydrogen phosphate aluminum, the products are PH_3 and H_2O in gas products. However, the thermal degradation of LHP and CHP occurs in three steps: dehydration, elimination of phosphine, and polycondensation. LOI and UL-94 tests showed that the metal hypophosphites AHP, LHP, and CHP can be used as effective flame retardants for PBT.

Acknowledgements The work was financially supported by the Natural Science Foundation of China (Grant No. 21306035 and Grant No. 21276059).

References

1. Li QF, Li B, Zhang SQ, Lin M. Investigation on effects of aluminum and magnesium hypophosphites on flame retardancy and thermal degradation of polyamide6. J Appl Polym Sci. 2012;125:1782–9.
2. Yang W, Hong NN, Song L, Hu Y, Yuen RKK, Gong XL. Studies on mechanical properties, thermal degradation, and combustion behaviors of poly(1,4-butyleneterephthalate)/glassfiber/cerium hypophosphite composites. Ind Eng Chem Res. 2012;51:8253–61.
3. Zhao B, Hu Z, Chen L, Liu Y, Liu Y, Wang YZ. A phosphorus-containing inorganic compound as an effective flame retardant for glass-fiber-reinforced polyamide 6. J Appl Polym Sci. 2011;119:2379–85.
4. Yang W, Tang G, Song L, Hu Y, Yuen RKK. Effect of rare earth hypophosphite and melamine cyanurate on fire performance of glass-fiber reinforced poly(1,4-butylene terephthalate) composites. Thermochim Acta. 2011;526:185–91.
5. Yang W, Yuen RKK, Hu Y, Lu HD, Song L. Development and characterization of fire retarded glass-fiber reinforced poly(1,4-butyleneterephthalate) composites based on a novel flame retardant system. Ind Eng Chem Res. 2011;50:11975–81.
6. Yang W, Song L, Hu Y, Lu HD, Yuen RKK. Enhancement of fire retardancy performance of glass-fibre reinforced poly(ethylene terephthalate) composites with the incorporation of aluminum hypophosphite and melamine cyanurate. Compos Part B. 2011;42:1057–65.
7. Tang G, Wang X, Xing WY, Zhang P, Wang BB, Hong NN, Yang W, Hu Y, Lei Song. Thermal degradation and flame retardance of biobased polylactide composites based on aluminum hypophosphite. Ind Eng Chem Res. 2012;51:12009–16.
8. Chuanmei J, Jinlong Z, Xilei C, Shaoxiang L. Flame retardant epoxy resin based on bisphenol A epoxy resin modified by phosphoric acid. J Therm Anal Calorim. 2013;114:253–9.
9. Jianzhong X, Zhanmeng H, Weihong W, Haiyun M, Jixing X, Hongqiang Q, Yunhong J. Study of thermal properties of flame retardant epoxy resin treated with hexakis[*p*-(hydroxymethyl)phenoxy]cyclotriphosphazene. J Therm Anal Calorim. 2013;114:1341–50.
10. Awad WH, Wilkie CA. Investigation of the thermal degradation of polyurea: the effect of ammonium polyphosphate and expandable graphite. Polymer. 2010;51:2277–85.
11. Shibin N, Chao P, Shujie Y, Mingxu Z. Thermal and flame retardant properties of novel intumescent flame retardant polypropylene composites. J Therm Anal Calorim. 2013;113:865–71.
12. Hongfei C, Qinfu L, Jing L, Bo S, Yanxia K, Ray LF. TG–MS–FTIR (evolved gas analysis) of kaolinite–urea intercalation complex. J Therm Anal Calorim. 2014;116:195–203.
13. José LF, Marta RB, César MS, Susana OE. Pyrolysis study of hydrophobic *tholins* By TG–MS, TG, DTA and DSC methods. J Therm Anal Calorim. 2013;111:1699–706.
14. Seddon JA, Jackson ARW, Kresiński RA, Platt AWG. Complexes of the lanthanide metals (La–Nd, Sm–Lu) with hypophosphite and phosphite ligands: crystal structures of $[Ce(H_2PO_2)_3(H_2O)]$, $[Dy(H_2PO_2)_3]$ and $[Pr(H_2PO_2)(HPO_3)(H_2O)]H_2O$. J Chem Soc Dalton Trans. 1999;21:89–96.
15. Soni BH, Deshpande MP, Bhatt SV, Chaki SH, Sathe V. X-ray diffraction, X-ray photoelectron spectroscopy and Raman spectroscopy of undoped and Mn-doped ZnO nanoparticles prepared by microwave irradiation. J Appl Spectro. 2013;79:901–7.
16. Noisong P, Danvirutai C, Srithanratana T, Boonchom B. Synthesis characterization and non-isothermal decomposition kinetics of manganese hypophosphite monohydrate. Solid State Sci. 2008;10:1598–604.
17. Yoshida Y, Inoue K, Kyritsakas N, Kurmoo M. Syntheses, structures and magnetic properties of zig-zag chains of transition metals. Inorg Chim Acta. 2009;362:1428–34.
18. Tanner PA, Faucher MD, Mak TCW. Synthesis, structure, and spectroscopy of rare earth hypophosphites. 1. Anhydrous and monohydrated lanthanide hypophosphites. Inorg Chem. 1999;38:6008–23.
19. Yang W, Song L, Yuan Hu, Lu HD, Yuen RKK. Investigations of thermal degradation behavior and fire performance of halogen-free flame retardant poly(1,4-butylene terephthalate) composites. J Appl Polym Sci. 2011;122:1480–8.
20. Qu HQ, Wu WH, Wu HJ, Xie JX, Xu JZ. Study on the effects of flame retardants on the thermal decomposition of wood by TG–MS. J Therm Anal Calorim. 2011;103:935–42.